Pergamon

J. Aerosol Sci. Vol. 30, No. 5, pp. 559–567, 1999

Printed in Great Britain

PII: S0021-8502(98)00753-8

0021-8502/99/$ - see front matter

POLAR STRATOSPHERIC CLOUDS OF LIQUID AEROSOL: AN EXPERIMENTAL DETERMINATION OF MEAN SIZE DISTRIBUTION

Marta Pantani,* Massimo Del Guasta,†‡ Donatella Guzzi† and Leopoldo Stefanutti†

* Fisbat-CNR, Via Gobetti 101, 40129 Bologna, Italy
† IROE-CNR "Nello Carrara", Via Panciatichi 64, 50127 Florence, Italy

(*First received* 6 *April* 1998; *and in final form* 25 *September* 1998)

Abstract—The determination of the mean size distribution for a Type Ib Polar Stratospheric Cloud ("PSC") has been performed for the first time using extinction/backscattering ratios as obtained from LIDAR data at 355, 532 and 750 nm. The multiwavelength Lidar was operated in Sodankyla, Finland, during the Second European Stratospheric Arctic and Middle-latitudes Experiment (SESAME, November 1994–April 1995). It produced vertical profiles of PSC. Log-normal distributions of supercooled ternary solution (STS), composed of H_2SO_4–HNO_3–H_2O particles with mode radius of 0.68–0.9 μm and standard deviation of 1.1–1.4, were retrieved as best fit to experimental data. Laboratory measurements of n_r (real part of refractive index), in the 404–633 nm range, show that it depends on the water/acid ratio without any distinction between binary and ternary solutions of nitric and sulphuric acid.

1. INTRODUCTION

Heterogeneous reactions on particles of polar stratospheric cloud (PSC) are central to the process of chlorine activation involved in ozone depletion. Two types of PSCs have been reported in the literature. The first type is further classified as types Ia, b, and c which are described, respectively, as large spherical nitric acid trihydrate (NAT) (Toon *et al.*, 1986; Crutzen and Arnold, 1986), small spherical ternary liquid solution of sulphuric and nitric acids, supercooled ternary solution (STS) (Carslaw *et al.*, 1994) and small non-spherical solid particles (metastable HNO_3, H_2O, Tabazadeh and Toon, 1996). Type II PSC are associated with water ice (Kent *et al.*, 1986).

Following the theory of Carslaw *et al.* (1994) and Drdla *et al.* (1994), PSC Ib seemingly occur when the air mass is initially at a temperature over the sulphuric acid trihydrate (SAT) melting point, and then passes below this point without ever reaching the ice frost point. In these conditions PSC formation occurs because of the growth of background sulphuric aerosol particles due to the absorption of water vapour and nitric acid. This process should be more efficient at temperatures close to the freezing point of water. The droplets are supposed to be composed of a ternary solution of nitric acid, sulphuric acid and water (STS). The concentrations of nitric acid and sulphuric acid in the droplets depend on the temperature.

In this paper, LIDAR measurements at three wavelengths have been used to retrieve the mean size distribution of a type Ib PSC measured during the Second European Stratospheric Arctic and Middle-latitudes Experiment (SESAME) campaign in Sodankyla, Finland (66°N). The cloud was observed on 19 January 1995 from 10 a.m. to 2 p.m.

The PSC backscattered signal was measured at three wavelengths, 355, 532, 750 nm, using a multispectral Lidar. The data inversion gave the wavelength dependence of both the integrated aerosol backscattering β_a and the extinction coefficient σ_a. The same optical quantities were simulated with a Mie code (Del Guasta, 1992) by varying the mode radius and the geometrical width of a log-normal distribution of STS particles of a differing

‡ Author to whom correspondence should be addressed.

chemical composition. A comparison between Lidar data and Mie simulations was carried out with χ^2 minimisation, in order to retrieve the composition and the particle size distribution of the PSC.

Since the wavelength-dependence of the refractive index used in the Mie code is a function of the composition of the STS, laboratory measurements of the refractive index of ternary solutions at different wavelengths and concentrations were performed with a spectrometer at 294 K. The corresponding refractive indexes at the PSC temperature of 190 K were calculated using the Lorenz–Lorenz formula.

Measurements showed that H_2SO_4–H_2O and HNO_3–H_2O solutions of the same weight concentrations have very similar refractive indices in the 404–633 nm spectral range; for concentrations of 0–60%, this is valid both at 294 and 190 K.

2. THE EXPERIMENTAL SET-UP

The Lidar system used during the "Measurements and modelling of Ozone and Aerosols in the Northern Atmosphere" (MOANA) experiment of the SESAME campaign was similar to the Lidar operated in Sodankyla during the European Arctic Stratospheric Ozone Experiment (EASOE), described in Stefanutti *et al.* (1992). The main difference was the simultaneous acquisition of all wavelengths.

Two lasers were used as transmitters:

(a) a Nd–YAG laser supplied with second- and third-harmonic generators, with a 10-pps repetition rate, 10 ns pulse length, 0.8-mr full-angle divergence, and pulse energies of about 320 mJ at 1064 nm, 500 mJ at 532 nm and 180 mJ at 355 nm;

(b) a Ti-sapphire laser having a 10-pps repetition rate, 50 ns pulse length and 0.8-mr full-angle divergence, with a 400 mJ output energy at 750 nm.

A 0.8-m-diameter telescope, with a 1.3-mr (full-angle) field of view and six detection channels, two of which cross-polarised, was used as receiver. Photomultipliers with S20 cathodes were used as detectors.

As supporter of the experiment two PTU (Pressure, Temperature, humidity) balloons were launched daily. In addition two backscattering sounds were launched by the Finnish Meteorological Institute on the same day as the PSC measurement. Such sounds, described by Larsen (1992), measured $\beta_{aj} + \beta_{mj}$, respectively, aerosol and molecular backscattering at wavelength j, at 173° scattering angle, for a volume of 1 m^3, at 490 and 940 nm.

2.1. *The PSC of* 19 *January* 1995

The cloud was observed on 19 January 1995, from 10 a.m. to 2 p.m. The cloud β_{aj} at 532 nm wavelength is reported in Fig. 1. The height resolution of the Lidar sounding was 75 m and the measurements were carried out every 10 min. The PSC showed a low integrated backscattering (about $2 \times 10^{-7}\ m^{-1}\ sr^{-1}$) and an optical depth in the 0.05–0.1 range. The Lidar signal did not show any aerosol depolarisation at 532 and 750 nm ($< 1\%$), it is characteristic of type Ib PSC. The absence of depolarisation made it possible to assume the presence of spherical liquid (Carslaw *et al.*, 1994; Drdla *et al.*, 1994) particles and to use Mie simulations. The temperature of the stratosphere was 190 K at 15 km.

At an altitude between 10 and 15 km, in the absence of PSC, a residual layer of Mount Pinatubo eruption was visible by means of the Lidar, with a peak value of β of about $0.5 \times 10^{-7}\ m^{-1}\ sr^{-1}$.

3. LIDAR DATA INVERSION

The method used for the Lidar data processing (Morandi, 1992) involves two boundary values, one above the cloud layer and another below. A constant cloud extinction-to-backscatter ratio K is then retrieved, as described below.

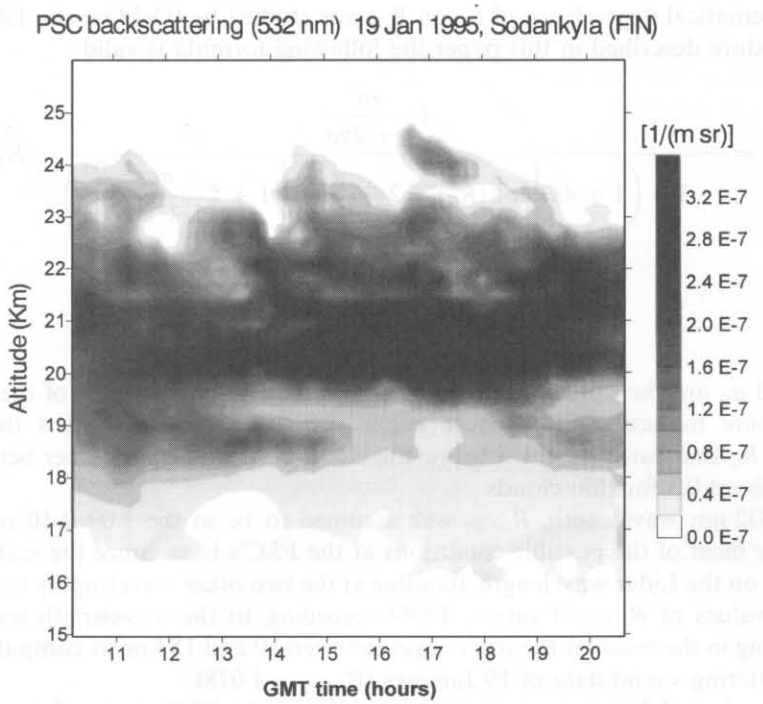

Fig. 1. Time–height evolution of 532 nm backscattering ratio of the cloud observed in Sodankyla (Finland), on 19 January 1995 from 10 a.m. to 2 p.m. Aerosol depolarisation was below 1% for the whole plot.

The PTU data closest in time to the LIDAR data is automatically searched, and the five coefficients of the molecular density fitting function

$$d(z) = \exp(c_1 + c_2 z + c_3 z^2 + c_4 z^3 + c_5 z^4) \tag{1}$$

are computed on the basis of the measured density profiles. In equation (1), d is the density ($\mathrm{kg\,m^{-3}}$) and z is the altitude. The density profile is then converted to the molecular backscatter profile. The Lidar signal is first calibrated with the molecular backscatter profile using two points above the cloud to solve the signal offset.

The scattering ratio is defined by

$$R_j = (\beta_{aj} + \beta_{mj})/\beta_{mj} \tag{2}$$

with β_{mj} the molecular backscattering at wavelength j, and β_{aj} the aerosol backscattering at wavelength j. R_j below the cloud base is called R_{0j}.

The square-range-corrected LIDAR return is converted into an attenuated backscatter profile by fitting the signal to R_{0j} times the molecular backscatter profile below the cloud base: because of the Mt. Pinatubo residual layer, below the cloud the value of R_{0j} is not known. When the particle loading is not negligible, $R_0 > 1$ must be used in the Lidar inversion algorithms. When no accessory data are available a guess for R_0 ($R_0 = 1$) is used and the error introduced in the Lidar profile will be corrected with the algorithm developed by Del Guasta (1998).

The relationship between the aerosol extinction $\sigma_{aj}(z)$ and the backscattering $\beta_{aj}(z)$ is assumed to be: $K_j\beta_{aj}(z) = \sigma_{aj}(z)$. R_j are assumed to be 1 above the cloud top. By using these scattering ratios and starting from arbitrary values of K_j, the inversion routine is iterated, with the value of K_j step varied, until a good agreement with the boundary conditions is reached in the same manner as done by Sassen and Cho (1992).

The PSC size distribution has been estimated by investigating the dependence on the wavelength of the extinction/backscattering ratio K_j.

The mathematical dependence of K_j on R_{0j} was studied by (Del Guasta, 1998). For the fitting procedure described in this paper the following formula is valid:

$$K = \frac{4\dfrac{\alpha\sigma}{1+2\alpha\sigma}}{-1+\left(1+4\alpha\left\{\log(R_0)+2\dfrac{\sigma}{1+2\alpha\sigma}\left[1+2\dfrac{\alpha\sigma}{1+2\alpha\sigma}\right]\right\}\right)^{1/2}} K_0,$$

where

$$\sigma = \sigma_0 - \frac{\log(R_0)}{2} \tag{3}$$

with K_0 and σ_0 are the optical parameters computed by the inversion of the Lidar data supposing pure molecular atmosphere below the cloud base, K and σ the corrected parameters, R_0 the scattering ratio below the cloud base, and α a number between 0 and 1 which is about 0.5 for thin clouds.

For the 532 nm wavelength, R_{0532} was assumed to be in the 1.00–1.10 range, which should cover most of the possible conditions at the PSC's base. Since the scattering ratio R_{0j} depends on the Lidar wavelength, its value at the two other wavelengths was computed for several values of R_{0532} (Pantani, 1996) according to the wavelength scaling of the backscattering in the residual Pinatubo layer between 10 and 15 km, as computed by using the backscattering sound data of 19 January ($R_{0532} = 1.078$).

A total number of 50 measurements were made on the PSC so that, for each value of R_{0532}, the Lidar data inversion provided a set of 50 values for each K_j.

Both K_{532} and K_{355} show a smaller statistical dispersion than K_{750}. As a consequence, the 532 nm and the 355 nm data play a major role in the least-squares method used to obtain the size distribution.

4. SCATTERING SIMULATION

PSC Ib are supposed to be composed by a ternary solution of HNO_3–H_2SO_4–H_2O (Carslaw *et al.*, 1994; Drdla *et al.*, 1994).

Simulations of the scattering by spherical aerosols were performed with a Mie code developed by Del Guasta (1992). A data set of backscattering and extinction efficiencies, at 355, 532 and 750 nm, as functions of the size parameter was produced for values of the refractive index corresponding to pure water and to several concentrations of H_2SO_4–H_2O and HNO_3–H_2O solutions (10, 30, 50 and 70%) at a temperature of 190 K.

The refractive index of binary solution H_2SO_4–H_2O at various wavelengths and concentrations was obtained at 300 K from the data of Palmer and Williams (1975). The imaginary part of the refractive index has been disregarded. Since no data on refractive indexes of HNO_3–H_2O and H_2SO_4–HNO_3–H_2O solutions has been found, they were experimentally measured.

The HNO_3–H_2O and H_2SO_4–HNO_3–H_2O solutions were prepared, with weight concentrations ranging from 10 to 60% for each acid. The refractive index of the prepared solutions at different wavelengths (404.7, 435.8, 546.1, 587.6 and 632.8 nm) was measured with a Pulfrich spectrometer (model PR2 made by Jenoptik Jena GmbH) at a temperature of 294 K (see Tables 1 and 2).

The refractive indexes were shifted to stratospheric temperatures by the Lorentz–Lorentz formula, as suggested by Steele and Hamill (1981):

$$n(T) = \left(\frac{2A\rho(T)+1}{1-A\rho(T)}\right)^{1/2}, \quad A = \frac{n^2(T_0)-1}{[n^2(T_0)+2]\rho(T_0)}, \tag{4}$$

where $n(T)$ is the refractive index at temperature T, $\rho(T)$ is the solution density at the same temperature, $n(T_0)$ is the refractive index at the reference temperature T_0 and $\rho(T_0)$ is the solution density at T_0.

Table 1. Refractive index of aqueous solution of nitric acid as a function of weight concentration at 404.7, 435.8, 546.1, 587.6 and 632.8 nm measured at 294 K

HNO_3 concentration (%)	Wavelength				
	404.7 nm	435.8 nm	546.1 nm	587.6 nm	632.8 nm
0	1.3426	1.34	1.3343	1.3322	1.3315
10	1.3558	1.3532	1.3466	1.345	1.3436
20	1.371	1.368	1.3606	1.3588	1.3572
30	1.3857	1.3821	1.3741	1.3721	1.37
40	1.399	1.3952	1.3865	1.3843	1.3823
50	1.4095	1.4054	1.3962	1.3939	1.3915
60	1.4114	1.4073	1.398	1.3958	1.3932

Table 2. Refractive index of ternary solution $H_2SO_4/HNO_3/H_2O$ as function of weight concentration for five wavelengths (404.7, 435.8, 546.1, 587.6 and 632.8 nm), measured at 294 K

Acid concentration		Wavelength				
$\%HNO_3$	$\%H_2SO_4$	404.7 nm	435.8 nm	546.1 nm	587.6 nm	632.8 nm
10	10	1.3704	1.3675	1.3608	1.3590	1.3575
10	20	1.3829	1.3798	1.3730	1.3713	1.3697
10	30	1.3930	1.3902	1.3832	1.3815	1.3798
10	40	1.4051	1.4020	1.3950	1.3932	1.3917
10	50	1.4179	1.4148	1.4078	1.4059	1.4040
20	10	1.3863	1.3831	1.3757	1.3737	1.3717
20	20	1.3968	1.3938	1.3862	1.3843	1.3826
20	30	1.4068	1.4037	1.3961	1.3942	1.3924
20	40	1.4179	1.4146	1.4071	1.4051	1.4034
30	10	1.3992	1.3956	1.3875	1.3855	1.3838
30	20	1.4076	1.4038	1.3957	1.3938	1.3918
30	30	1.4169	1.4136	1.4056	1.4036	1.4017
40	10	1.4099	1.4062	1.3974	1.3952	1.3933
40	20	1.4166	1.4129	1.4045	1.4025	1.4005
50	10	1.4171	1.4132	1.4040	1.4023	1.3998

Table 3. Refractive index of binary solution HNO_3/H_2O, H_2SO_4/H_2O as a function of weight concentration at 355, 532 and 750 nm shifted at 190 K

λ (nm)	Acid	Acid concentration					
		0%	10%	20%	30%	50%	70%
355	HNO_3	1.311	1.3498	1.3839	1.4133	1.4757	1.4832
355	H_2SO_4	1.311	1.3675	1.395	1.417	1.452	1.474
532	HNO_3	1.3004	1.3364	1.3677	1.3945	1.4345	1.457
532	H_2SO_4	1.3	1.3525	1.375	1.394	1.43	1.431
750	HNO_3	1.2972	1.3305	1.359	1.3831	1.4181	1.4366
750	H_2SO_4	1.297	1.347	1.371	1.388	1.42	1.444

Density data $\rho(T_0)$ of binary solutions of HNO_3–H_2O at 294 K were obtained from Wolf *et al.* (1973). The density, at lower temperatures, was obtained from Kharbanda *et al.* (1956). The density of HNO_3 was shifted to 190 K (temperature of the January 19 PSC) with a linear interpolation (Beyer *et al.*, 1996). For concentrations of less than 20%, the density at 190 K was obtained from a linear interpolation between pure water and 20% acid density. For H_2SO_4, the density at 190 K was obtained from Steele and Hamill (1981).

At 190 K the difference between the real refractive index of nitric acid and sulphuric acid at the same weight concentration was less than 0.02 in the whole concentration range and spectral range (Table 3). An accuracy much better than 0.02 on the refractive index was thus necessary for determining which acid solution was present in the PSC aerosol. For a ternary

solution, a refractive index comprised between the two binary solutions, as suggested by Luo *et al.* (1996) was assumed.

Simulations of K_j were performed for the three LIDAR wavelengths. Monomodal log-normal distributions of the form:

$$N(r) = \frac{N_t}{\sqrt{2\pi}\, r \ln(s)} \exp\{-0.5[\ln(r/r_m)/\ln(s)]^2 \quad (5)$$

were used to model the stratospheric PSCs aerosol, where r_m was the mode radius, s was the width of the distribution and N_t was the total number concentration.

Scattering simulations for monomodal distributions were performed by changing r_m and s. A database of simulated aerosol backscatter (β_{sj}), extinction (σ_{sj}) and K_{sj} for a single particle ($N_t = 1$) was produced by varying r_m and s with steps of 0.02 μm for r_m and of 0.02 for s. The parameters r_m and s were varied between 0 and 2 μm and between 1.1 and 2, respectively.

Archive files containing these simulations were produced for pure water, binary and ternary solutions with acids in the 10–70% weight concentration range.

5. SIZE DISTRIBUTION RETRIEVAL METHOD

By processing each multiwavelength PSC measurement, the optical quantities $\beta_{aj}(z)$, $\sigma_{aj}(z)$ and K_j were obtained for different hypotheses on the value of R_{0532}.

The fundamental advantage in using K_j for the size retrieval is that it does not depend on the aerosol droplets density in the single-scattering approximation. This was a good approximation for the optical thin cloud of 19 January 1995. Mean values of K_j, therefore, could be computed by averaging the values retrieved from many LIDAR profiles, regardless of temporal changes in the cloud profile, assuming that the aerosol scattering properties did not change with time.

The experimental mean values of K_j (with the associated sample standard deviation ΔK_j) are listed in Table 4 for the hypothesis $1.00 < R_{0532} < 1.10$. These mean values were obtained (Pantani, 1996) by processing the whole set of Lidar data.

Searching for the best fitting size distribution, we performed a comparison between simulated and experimental K_j. The least-squares method was used to search for the minimum of the χ^2 function: χ^2 (R_0, acid concentration, r_m, s) $= \sum_{j=0}^{3} [(K_j - K_{sj})/\Delta K_j]^2$ where K_j are reported in Table 4 as a function of R_{0532} and K_{sj} have been simulated with a Mie code as a function of acid concentration, r_m and s. The same procedure was used by Del Guasta *et al.* (1994) to retrieve the size distribution of Pinatubo aerosol.

Figures 2 and 3 show the sections of χ^2 surface for $R_{0532} = 1.08$ and acid concentration of 30 and 50%, respectively. In those sections are visible the absolute minimum of χ^2 corresponding to the distributions summarised in Table 5.

The $\chi^2(r_m, s)$ surface for $R_{0532} = 1.08$ and 30% of nitric acid is shown in Fig. 2, demonstrating that the estimation errors on r_m and s were correlated negatively because of the linear shape of the bottom of the χ^2 surface. An error of $+0.1$ μm on the retrieved r_m led to an error of approximately -0.15 on s.

Table 4. Experimental values of K_j at different R_{0j} computed using Del Guasta (1998)

Wavelength (nm)	$R_{0532} = 1.00$	$R_{0532} = 1.02$	$R_{0532} = 1.04$	$R_{0532} = 1.06$	$R_{0532} = 1.08$	$R_0 = 1.10$
355	23 ± 7	21 ± 7	19 ± 7	17 ± 7	16 ± 7	14 ± 7
532	43 ± 10	36 ± 10	30 ± 10	23 ± 11	17 ± 11	10 ± 11
750	160 ± 50	130 ± 50	100 ± 60	70 ± 60	50 ± 60	10 ± 60

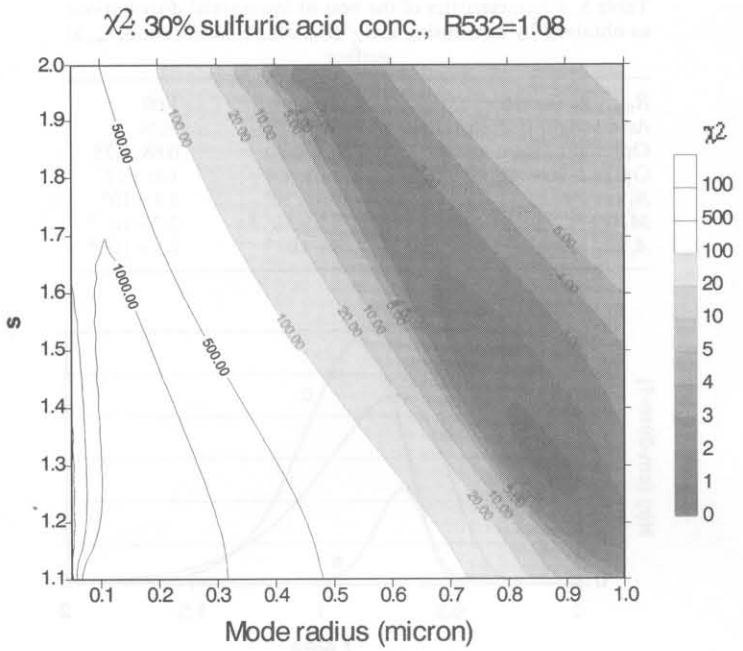

Fig. 2. Section of the $\chi^2(R_0$, acid concentration, r_m, $s)$ surface for 30% sulphuric (or nitric) acid concentration droplets and $R_0 = 1.08$ below the cloud base, resulting from experimental K_j and simulated K_{sj}. The bottom is well defined at 0.8–0.9 μm modal radius, $s = 1.3$–1.4.

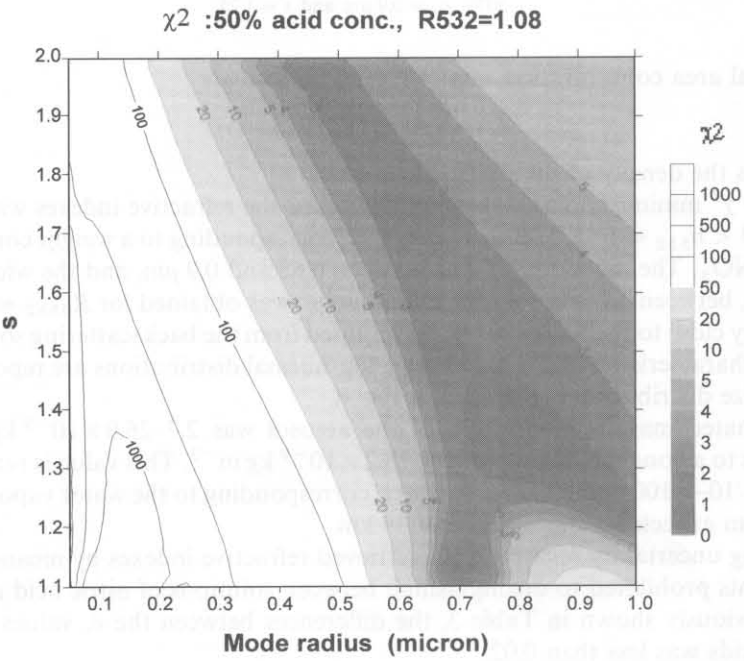

Fig. 3. Section of the $\chi^2(R_0$, acid concentration, r_m, $s)$ surface for 50% sulphuric (or nitric) acid concentration droplets and $R_0 = 1.08$ below the cloud base, resulting from experimental K_j and simulated K_{sj}. The bottom is well defined at 0.68–0.75 μm modal radius, $s = 1.1$–1.15.

Knowing the (r_m, s) optimal pair, from the simulated $\beta_{sj}(r_m, s)$ and from the measured β_{aj} it was possible to find the total number density of particles N_t: $N_t \approx \beta_{sj}/\beta_{sj}$. The total aerosol mass concentration was

$$M_t = \rho N_t \tfrac{4}{3}\pi r_m^3 \exp[\tfrac{9}{2}\log^2(s)] \quad (6)$$

Table 5. Characteristics of the best-fit log-normal distributions as obtained by minimising the $\chi^2(R_0$, acid concentration, r_m, $s)$ surface

R_{0532} at the cloud base	1.08	1.08
Acid weight concentration	30%	50%
Optimal r_m (μm) range	0.8; 0.9	0.68; 0.75
Optimal s range	1.25; 1.4	1.1; 1.15
N_t (m^{-3})	5.7×10^6	1.1×10^6
M_t ($kg\,m^{-3}$)	2.6×10^{-8}	2.7×10^{-9}
A_t ($m^2\,m^{-3}$)	9×10^{-5}	8.5×10^{-6}

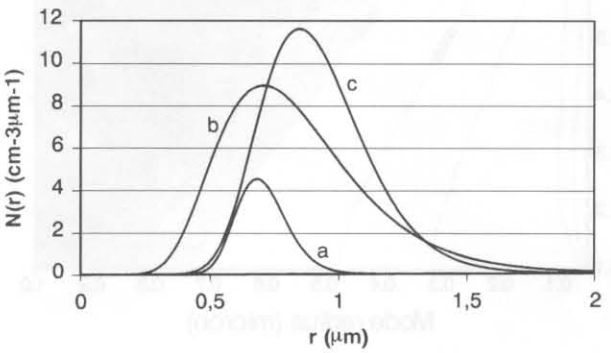

Fig. 4. Best-fit log-normal distributions as obtained by minimising the χ^2 (R_0, acid concentration, r_m, s) surface. $N(r) = [N_t/\sqrt{2\pi}r\ln(s)]\exp\{-0.5[\ln(r/r_m)/\ln(s)]^2$, with $N(r)$ ($cm^{-3}\,\mu m^{-1}$), r_m (μm) and s taken from Table 5. Curve (a) is for an acid concentration of 50%, $r_m = 0.7$ μm and $s = 1.15$, (b) for an acid concentration of 30%, $r_m = 0.8$ μm and $s = 1.4$ and (c) for an acid concentration of 30%, $r_m = 0.9$ μm and $s = 1.25$.

and the total area concentration was

$$A_t = N_t 4\pi r_m^2 \exp[2\log(s)], \tag{7}$$

where ρ was the density of the particle.

From the χ^2 minimisation, the best matching for the refractive indexes was $1.41 < n_{355} < 1.47$, $1.39 < n_{532} < 1.43$, $1.38 < n_{750} < 1.42$, corresponding to a weight concentration of 30–50% HNO_3. The mode radius was between 0.65 and 0.9 μm, and the width of the size distribution, between 1.1 and 1.4. The minimum χ^2 was obtained for $R_{0532} = 1.08$, a figure that was very close to the $R_{0532} = 1.078$ computed from the backscattering sound (Pantani, 1996). The characteristics of the best-fitting, log-normal distributions are reported in Table 5 and the size distribution is reported in Fig. 4.

The estimated mass concentration of the aerosol was $2.7–26.0 \times 10^{-9}\,kg\,m^{-3}$, which corresponds to a condensed water of $1.3–18.2 \times 10^{-9}\,kg\,m^{-3}$. This value is reasonable, as it was about 1/10–1/100 of the available water, corresponding to the water vapour concentration of 5 ppm expected at an altitude of 19 km.

The strong uncertainty regarding the retrieved refractive indexes by means of the Lidar measurements prohibited to distinguishing between solutions of nitric acid and sulphuric acid; as previously shown in Table 3, the differences between the n_r values of nitric and sulphuric acids was less than 0.02.

The retrieved acid concentration range was comparable to that obtained by an analysis of the thermal history of different air masses reaching Sodankyla during the Lidar measurements (Rizi *et al.*, 1995). The results of the simulation show a PSC acid concentration of 40% in weight for HNO_3 and less than 1% for H_2SO_4.

6. CONCLUSIONS

The use of Lidar-derived multiwavelength extinction/backscattering ratio showed itself to be a promising method for the remote measurement of the size distribution of liquid

stratospheric aerosols. By using this method, the Lidar-derived size distribution of a liquid PSC was estimated for the first time to our knowledge.

The measurements at 190 K of the real refractive index of nitric acid and sulphuric acid at the same weight concentration showed a small change in the refraction index with the change of the chemical composition. The uncertainty in determining the refractive index of PSC particles by means of a visible Lidar does not at present permit a distinction between binary and ternary solutions of nitric and sulphuric acid.

The best fit of experimental data showed a log-normal distribution of particles with mode radius of $r_m = 0.65$–$0.9\ \mu$m, width of $s = 1.1$–1.4, mass concentration of 2.7–$26.0 \times 10^{-9}\ \mathrm{kg\,m^{-3}}$, and a weight concentration of 30–50% HNO_3. The best matching for the refractive indexes was $1.41 < n_{355} < 1.47$, $1.39 < n_{532} < 1.43$, $1.38 < n_{750} < 1.42$.

The method gave meaningful results when the particle size was almost uniform within the cloud. The size distribution shape should also be constant or slowly varying with time, because it is necessary to average K_j values coming from Lidar profiles taken at different times in order to obtain reliable mean K_j values. K_j are, in fact, affected by large errors resulting from the natural fluctuations of K_{0j}, σ_0 and R_{0j}. The uncertainly on K_{0j} and σ_0 is mainly due to the change of the cloud during the measurement time and it is a statistic error estimated from the data set. The uncertainty on R_{0j} is mainly due to the error on the wavelength scaling on the backscattering in the residual Pinatubo layer computed from backscattering sound data. In the case of the 19 January PSC the error computation shows that the main contribution to the error on K_j is due to the fluctuation of K_{0j}.

REFERENCES

Beyer, K. D., Ravishankara, A. R. and Lovejoy, E. R. (1996) *J. Geophys. Res.* **101,** 14,519–14,524.

Carslaw, K. S., Luo, B. P., Clegg, S. L., Peter, T. H., Brimblecombe P. and Crutzen, P. J. (1994) *GRL* **21,** 2479–2482.

Crutzen, P. J. and Arnold, F. (1986) *Nature* **324,** 18–25.

Del Guasta, M. (1992) A FORTRAN code for quick computing of light scattered by spherical particles, with particular reference to backscattering LIDAR. *CNR Rep. TR/GCF/91.22* (Istituto di Ricerca sulle Onde Elettromagnetiche, Firenze, Italy).

Del Guasta, M., Morandi, M., Stefanutti, L., Stein, B. and Wolf, J. P. (1994) *Appl. Opt.* **33,** 5690–5697.

Del Guasta, M. (1998) *Appl. Opt.* 37, 24, 5522–5540.

Drdla, K., Tabazadeh, A., Turco, R. P., Jacobson, M. Z., Dye, J. E., Twohy, C. and Baumgardner, D. (1994) *GRL* **21,** 2475–2478.

Kent, G. S., Poole, L. R. and McCormick, M. P. (1986) *J. Atmos. Sci.* **43,** 2149–2161.

Kharabanda, N. (1956) *Ind. Chemist.* **32,** 412–413.

Larsen, N. (1992) Stratospheric aerosols: backscatter measurements from Thule European Arctic Stratospheric Ozone Experiment. *Danish Meteorological Institute, Scientific Report 92-1,* Copenhagen.

Luo, B., Krieger, U. and Peter, T. (1996) *Geophys. Res. Lett.* **23,** 3707–3710.

Morandi, M. (1992) A complete procedure for inverting backscattering LIDAR returns. *Research Rep. RR/GCF/92.11* (Istituto di Ricerca sulle Onde Elettromagnetiche, Firenze, Italy).

Palmer, K. F. and Williams, D. (1975) *Appl. Opt.* **14,** 208–219.

Pantani, M. (1996) Studio di Nubi Polari Stratosferiche mediante Lidar multispettrale. *Tesi di laurea in Fisica,* Università degli studi di Firenze, Corso di Laurea in Fisica.

Rizi, V., Redaelli, G., Visconti, G., Masci, F., Ivanova, I., Wedekind, C., Immler, F., Mielke, B., Rairoux, P., Stein, B., Woste, L., Del Guasta, M., Morandi, M., Stefanutti, L., Matthey, R., Mitev, V., Douard, M., Wolf, J. P., Kiro, E. and Kivi, R. (1995) A case study during SESAME. *3rd European Symp. on Polar Stratospheric Ozone Research,* Schliersee, Germany, 18–22 September.

Sassen, K. and Cho, B. S. (1992) *J. Appl. Meteorol.* **31,** 1275–1285.

Steele, H. M. and Hamill, P. (1981) *J. Atmos. Sci.* **12,** 517–528.

Stefanutti, L., Castagnoli, F., Del Guasta, M., Morandi, M., Sacco, V. M., Venturi, V., Zuccagnoli, L., Kolenda, J., Kneipp, H., Rairoux, P., Stein, B., Weidaner, D. and Wolf, J. P. (1992) *Appl. Phys. B* **55,** 13–17.

Tabazadeh, A. and Toon, O. B. (1996) *J. Geophys. Res.* **101,** 9071–9078.

Toon, O. B., Hamill, P., Turco, R. P. and Pinto, J. (1986) *GRL* **13,** 1284–1287.

Wolf, A. V., Horten, G., Brown, G. and Prentiss, G. (1973) *Handbook of Chemistry and Physics,* 54th Edition, OH, D271 D247 Ed. CRC, Cleveland.